Zhang *et al. Microstructures* 2024;4:2024002
DOI: 10.20517/microstructures.2023.63

Microstructures

Research Article

Open Access

Check for updates

First-principles study on the negative/zero area compressibility in Ag_3BO_3 with "wine-rack" architecture

Xingyu Zhang[1,3], Youquan Liu[1,3], Naizheng Wang[1,3], Xingxing Jiang[1,2], Zheshuai Lin[1,2]

[1]Functional Crystals Lab, Technical Institute of Physics and Chemistry, Chinese Academy of Sciences, Beijing 100190, China.
[2]Center of Materials Science and Optoelectronics Engineering, University of Chinese Academy of Sciences, Beijing 100049, China.
[3]University of the Chinese Academy of Sciences, Beijing 100049, China.

Correspondence to: Prof. Xingxing Jiang, Functional Crystals Lab, Technical Institute of Physics and Chemistry, 29 Zhongguancun East Road, Haidian District, Beijing 100190, China. E-mail: xxjiang@mail.ipc.ac.cn; Prof. Zheshuai Lin, Functional Crystals Lab, Technical Institute of Physics and Chemistry, 29 Zhongguancun East Road, Haidian District, Beijing 100190, China. E-mail: zslin@mail.ipc.ac.cn

How to cite this article: Zhang X, Liu Y, Wang N, Jiang X, Lin Z. First-principles study on the negative/zero area compressibility in Ag_3BO_3 with "wine-rack" architecture. *Microstructures* 2024;4:2024002. https://dx.doi.org/10.20517/microstructures.2023.63

Received: 25 Oct 2023 **First Decision:** 14 Nov 2023 **Revised:** 20 Nov 2023 **Accepted:** 12 Dec 2023 **Published:** 2 Jan 2024

Academic Editor: Andrea Sanson **Copy Editor:** Fangling Lan **Production Editor:** Fangling Lan

Abstract

Materials with negative/zero area compressibility (NAC or ZAC), which expand or keep constant along two directions under hydrostatic pressure, are very rare but of great scientific and engineering merits. Here, we investigate "wine-rack" architecture, which is the most prevailing for the pressure-expansion effect in materials, and identify that two allotropes (Ag_3BO_3-*I* and -*II*) of Ag_3BO_3 have the ZAC and NAC effects, respectively, by the first-principles calculations. Structural analysis discloses that the competition between the contraction effect from the bond length/angle shrinkage and the expansion effect from the angle closing between O-Ag-O bars and the (*a*, *b*) plane dominates the occurrence of ZAC/NAC, and the framework openness governs the competing balance in this system. This work deepens the understanding of "wine-rack" models and enriches the NAC/ZAC family.

Keywords: Negative area compressibility, zero area compressibility, wine-rack, borate

INTRODUCTION

It is well-recognized that materials would contract along three dimensions when being squeezed under hydrostatic pressure[1]. However, very few materials would abnormally expand or remain constant along one or two directions as hydrostatic pressure increases, which is termed negative or zero compressibility[2-5]. These counterintuitive pressure-responding behaviors bring great application prospects in many fields, such as shock wave absorption[6,7], body armor[8,9], ultrasensitive pressure detectors[3,5,10], deep-sea optical cable[11,12], *etc*. The exploration of these anomalous mechanical materials has been one of the most advanced branches of mechanical functional materials. From the viewpoint of occurring dimensions, the anomalous compressibility can be categorized into negative/zero linear compressibility (NLC/ZLC)[13,14], negative/zero area compressibility (NAC/ZAC)[11,15,16], and negative/zero volume compressibility (NVC/ZVC)[17-19]. Due to the restrictions imposed by thermodynamical laws, the NVC behavior can only occur alongside phase transitions[17,18], which are forbidden in dynamically stable systems. Meanwhile, ZVC only appears in highly dense-packed structure materials, such as diamond[19], in which an extremely difficult synthesis condition is required. Therefore, the materials with one/two-dimensional anomalous compressibility become the ideal choice for the application. Compared with NLC or ZLC, NAC/ZAC has a greater advantage in the device where highly dimensional pressure-driven expansion is required, with the example of shock-resistant optical windows[11] and ultra-precise ferroelectric pressure sensors[3]. However, due to the same reason, NAC/ZAC is much more scarcely occurring in comparison with NLC/ZLC, and the exploration of NAC/ZAC materials is a very challenging but highly desired issue.

In the past decades, much great effort has been devoted to the investigation of the structure-property relationship of NAC/ZAC, and several structural models have been proposed to elaborate the microscopic mechanism, such as "wine-rack" models[7,20,21], "helical chain" structures[3], and Lifshits mechanisms[22], which have strongly promoted the exploration of abnormal compressibility materials. Among them, the "wine-rack" motif, established on the bar-hinge model, is the most prevailing mechanism of these fascinating mechanical behaviors, which has led to the discovery of anomalous compressibility in dozens of materials, including $Ag_3Co(CN)_6$[23], $KMn[Ag(CN)_2]_3$[24], methanol monohydrate[25], MIL-53(Al)[20], MIL-122(In)[7], *etc*. Nonetheless, almost all these ever-discovered negative compressibility (NC) originating from the "wine-rack" motif only occur along one direction, and no NAC material has been detected by this structural prototype. In fact, the detailed strain-stress analysis on the building block bar of "wine-rack" architecture shows that the rotation direction of the bar strongly depends on its initial orientation in the structure: when the angle between bars and principal axis (*i*-axis) is smaller than 45°, the bar would rotate toward the principal axis and result in the NC along this direction [Figure 1A]; otherwise, it would rotate to the vertical axis and lead to NC along the vertical directions (*j*-axis) [Figure 1B]. Therefore, controlling the alignment angle of the bars in "wine-rack" structures is the key to modulating the direction of NC, which may promote the occurrence of NAC.

Planar coordination groups, such as $[BO_3]^{3-}$, $[CO_3]^{2-}$, and $[NO_3]^-$, can be considered to be dimensionless along the direction perpendicular to the plane, with which a small angle is possible generated so as to satisfy the structure requirement of the ZAC/NAC governed by "wine-rack" motif. Here, the $[BO_3]$ system is chosen to perform the structural screening. By connecting with the adjacent polyhedral units, $[BO_3]$ groups have constructed many crystals with anomalous pressure-responding properties, such as $KBe_2BO_3F_2$[16], $LiBO_2$[5], AEB_2O_4[26], *etc*. In this work, by adopting the first-principles simulations, we predict that two allotropes of Ag_3BO_3, Ag_3BO_3-*I* and -*II*, with "wine-rack" architecture in the $[BO_3]$ system exhibit the ZAC and NAC behaviors, respectively. The relationship between the geometrical configuration and the ZAC/NAC-occurring direction of the "wine-rack" structure is systematically discussed. It is revealed that NAC/ZAC in these two structures is attributed to the dominant effect from the bar rotation under pressure, and the opening angle within the bars determines whether NAC or ZAC occurs.

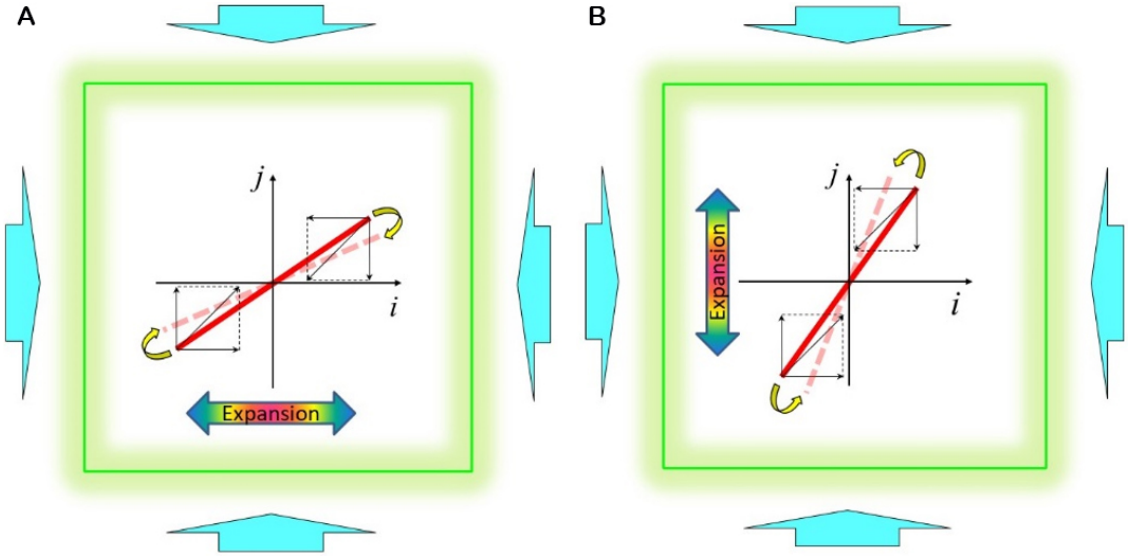

Figure 1. The mechanical analysis of the bar in "wine-rack" structures for the two conditions of the angle between the bar and principal axis (*i*-axis). (A) The condition for the angle smaller than 45°, in which the hydrostatic pressure results in a torque to drive the bar rotate toward the *i*-axis; (B) The condition for an angle larger than 45°, in which the hydrostatic pressure results in a torque to drive the bar rotate to be away from the *i*-axis. The rotation direction of the bar is highlighted by yellow arrows.

MATERIALS AND METHODS

The first-principles calculation was performed by the CASTEP[27], a program based on the plane-wave pseudopotential density functional theory (DFT)[28]. The functionals developed by Ceperley, Alder, Perdew, and Zunger (CA-PZ) in the form of local density approximation (LDA)[29,30] were chosen to model the exchange-correlation energy. The ultrasoft pseudopotentials[31] were used to describe the effective interaction between the atomic cores and valence electrons. Plane-wave energy cutoff was set to 400 eV, and the Monkhorst k-point mesh spanning less than 0.03 $Å^3$ was adopted. To get pressure-dependent crystal structures, the hydrostatic pressure was exerted from 0 to 10 GPa, and crystal structures were geometrically optimized by Broyden-Fletcher-Goldfarb-Shanno (BFGS) scheme[32], and the convergence criterion for energy, maximum force, maximum stress, and maximum displacement were set to 5×10^{-6} eV/atom, 0.01 eV/Å, 0.02 GPa, and 5×10^{-4} Å, respectively. The validity of first-principles calculation has been verified in some other anomalous mechanical materials, such as $LiBO_2$[5] and $[C(NH_2)_3][Cd(HCOO)_3]$[12]. The number of steps for each strain and the maximum strain amplitude were set to 6 and 0.002 to calculate elastic constants. Finally, based on the theoretical cell parameters, the PASCal[33] program developed by Cliffe *et al.* was used to fit the compressibility along the mechanical principal axes[33].

RESULTS AND DISCUSSION

The structures of Ag_3BO_3 were first determined by Jansen *et al.* and have two phases with the trigonal space group of *R*32 and *R*-3*c*, termed as Ag_3BO_3-*I* and Ag_3BO_3-*II*, respectively[34,35]. As shown in Figure 2A and B, Ag_3BO_3-*I* and Ag_3BO_3-*II* share a similar atomic configuration. In both two structures, one boron atom was coordinated with three oxygen atoms to construct the planar $[BO_3]$ triangles arranged parallel to the (*a*, *b*) plane. Silver atoms are bonded with two oxygen atoms to form two-fold coordinated bars of O-Ag-O. By sharing the ligand oxygen atoms, the O-Ag-O bars are further connected with the adjacent interlayer $[BO_3]$, giving rise to a "wine rack"-like structure. Accordingly, the lengths of the *a*- and *c*-axes are determined by the sum of the projection of the O-Ag-O bar along the *a*-axis combined with the size of $[BO_3]$ groups and the projection of the O-Ag-O bar along the *c*-axis, respectively. Interestingly, the O-Ag-O bars manifest the

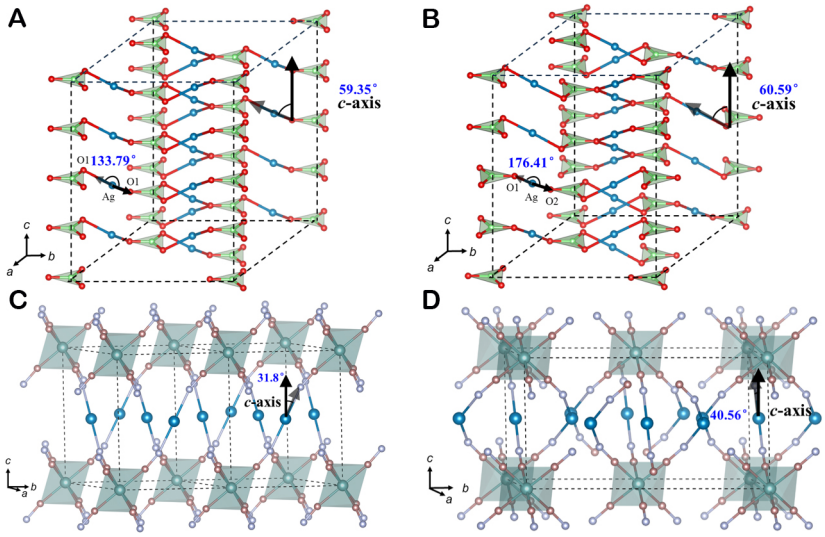

Figure 2. The crystal structure of $AgBO_3$ and $Ag_3Co(CN)_6$ (A) $AgBO_3$-*I*; (B) $AgBO_3$-*II*. (C) $Ag_3Co(CN)_6$-*I*; (D) $Ag_3Co(CN)_6$-*II*. The blue, green, red, grey, and brown balls are represented by Ag, B, O, N, and C atoms, respectively.

different configurations in these two structures. In Ag_3BO_3-*I*, the O-Ag-O bar is prominently distorted, and the angle of ∠O-Ag-O is 133.79°, while the counterpart in Ag_3BO_3-*II* manifests a more linear configuration and the angle of ∠O-Ag-O is 176.41°. Meanwhile, Ag_3BO_3-*I* has one symmetrically independent oxygen atom (O1), while two (O1 and O2) are contained in Ag_3BO_3-*II* due to the different space groups.

Both Ag_3BO_3-*I* and Ag_3BO_3-*II* have a similar "wine-rack" structure constructed by the O-Ag-O bars, as the CN-Ag-CN ones in $Ag_3Co(CN)_6$ [Figure 2C and D]. However, different from the hexagonal configuration of $[CoC_6]$ in $Ag_3Co(CN)_6$, the planar $[BO_3]$ groups in Ag_3BO_3-*I* and Ag_3BO_3-*II*, serving as the hinges of the "wine-rack" motif, are almost aligned along the (*a*, *b*) plane. Such a planar hinge configuration induces a more slant alignment of the bars with respect to the *c*-axis, and the angles between the O-Ag-O bar and *c*-axis in Ag_3BO_3-*I* and in Ag_3BO_3-*II* were 59.35° [Figure 2A] and 60.59° [Figure 2B], respectively, in comparison with the value of 31.8° [Figure 2C] and 40.56° [Figure 2D] in $Ag_3Co(CN)_6$-*I* and $Ag_3Co(CN)_6$-*II*[23]. According to the abovementioned mechanical analysis, it is anticipated that the conversion of the inclination angle across 45° from $Ag_3Co(CN)_6$ to Ag_3BO_3 might reverse the inclination direction of the bars and result in the expansion along the (*a*, *b*) plane under pressure.

To verify these postulations, first-principles calculations based on DFT are implemented to investigate the compressive behavior of Ag_3BO_3-*I* and Ag_3BO_3-*II*. In the first step, to confirm the validity of the DFT strategy on "wink-rack"-type structures, the calculation on the compressibility of $Ag_3Co(CN)_6$ was performed. As plotted in Figure 3A and B, and Supplementary Figure 1, regardless of a higher theoretical phase-transition pressure (3 GPa) than the observed values (0.19 GPa), both the NLC behavior and phase transition from *P*-31*m* to *C*2/*m* space groups in $Ag_3Co(CN)_6$ is reproduced [Supplementary Table 1]. This confirms the feasibility of our calculating methods. As shown in Figure 3C and D, no discontinuity of the enthalpy and the cell parameters emerge as pressure mounts from 0 to 10 GPa, indicating the absence of phase transitions and the high mechanical stability of both the two phases. In the pressure range of 0-10 GPa, the enthalpy of Ag_3BO_3-*II* is always smaller than that of Ag_3BO_3-*I*. Since the enthalpy difference between the two phases is 51.48 meV per atom, corresponding to the elementary excitation at 199.1 K per vibration freedom, one cannot distinguish which is more stable at room temperature (300 K). According to

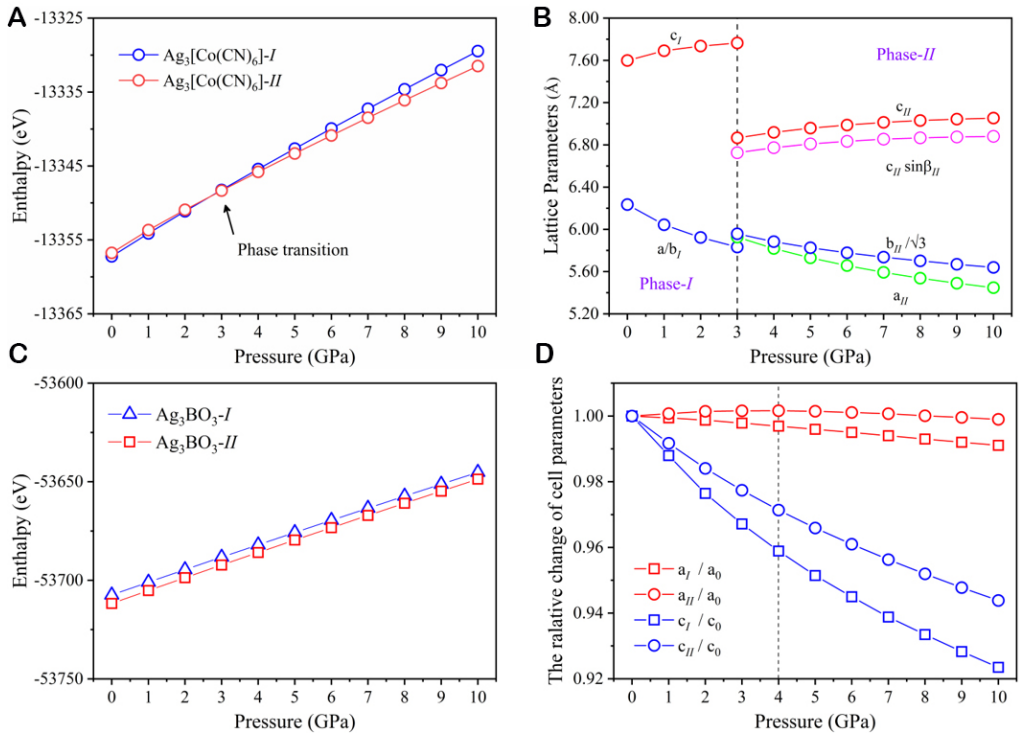

Figure 3. The calculated enthalpy and variation of cell parameters in $Ag_3Co(CN)_6$ and Ag_3BO_3 *vs.* pressure. (A) Pressure-dependent enthalpy for the low and high-pressure phases of $Ag_3Co(CN)_6$. (B) Pressure-dependent cell parameters of $Ag_3Co(CN)_6$. (C) Pressure-dependent enthalpy in Ag_3BO_3-*I* and Ag_3BO_3-*II*. (D) The relative change of pressure-dependent cell parameters in Ag_3BO_3-*I* and Ag_3BO_3-*II*. By considering the different numbers (*Z* value) of chemical formulas in the two phases of $AgBO_3$ and $Ag_3Co(CN)_6$, the enthalpies of $AgBO_3$-*I* and $Ag_3Co(CN)_6$-*I* are multiplied by the factor of 4 and 2, respectively.

the theoretical cell parameters, it is observed that the *a*/*b*-axis of Ag_3BO_3-*I* decreases from 9.97276 to 9.88381 Å (by -0.089%), and the *c*-axis decreases from 3.01461 to 2.84532 Å (by -5.6%) as pressure increases 0-10 GPa [Figure 3D and Supplementary Figure 2, Supplementary Table 2]. The compressibilities, fitted by the PASCal program[33], are 0.97 (1) TPa^{-1} and 4.95 (11) TPa^{-1} [Supplementary Figure 3] along the principal mechanical X_3- and X_1-axes (Transformation matrix was shown in Supplementary Table 3). The linear compressibility along the X_1-axis is of a similar magnitude to that of diamond (0.71 TPa^{-1}), so Ag_3BO_3-*I* is a material with extremely limited ZAC. Different from Ag_3BO_3-*I*, the *a*/*b*-axis of Ag_3BO_3-*II* abnormally expands from 9.94640 to 9.96232 Å (by 0.016%), and the *c*-axis decreases from 12.33943 to 11.83234 Å (by -4.11%) with the pressure increasing from 0 to 4 GPa [Figure 3D and Supplementary Figure 2, Supplementary Table 2]. The compressibilities along X_1 and X_3-axes are fitted to be -0.24 (22) TPa^{-1} and 9.26 (79) TPa^{-1}, respectively [Supplementary Figure 3, Supplementary Table 3], which demonstrates that Ag_3BO_3-*II* presents a NAC behavior with an area compressibility of -0.48 (44) TPa^{-1} within (*a*, *b*) plane [Supplementary Figure 4]. The observation of NAC in Ag_3BO_3-*II* is the first case in the "wine-rack" system. Above 4 GPa, as the pressure increases sequentially to 10 GPa, the *a*/*b*-axis and *c*-axis are inversed to shrink from 9.96232 to 9.93624 Å (by -0.26%) and from 11.83234 to 11.39554 Å (by -3.7%), and the linear compressibility along the principal mechanical X_3- and X_1-axis in this pressure range are 0.53 (2) TPa^{-1} and 5.51 (3) TPa^{-1} respectively. Accordingly, analogous to Ag_3BO_3-*I*, ZAC was also shown in Ag_3BO_3-*II*, with an area compressibility of 1.06 (4) TPa^{-1} within the (*a*, *b*) plane. To make a comparison with Ag_3BO_3-*I*, the compressibility of Ag_3BO_3-*II* in the whole pressure range (0~10 GPa) was fitted as well, and the linear compressibilities of X_3- and X_1-axes were 0.09 (14) TPa^{-1} and 6.56 (21) TPa^{-1}, respectively [Supplementary Figure 3 and Supplementary Table 3], both of which are similar with the ones of Ag_3BO_3-*I*.

Due to the similar cell parameter change in response to pressure, Ag_3BO_3-*I* and Ag_3BO_3-*II* share a similar mechanical property, especially for the bulk modulus, 101.55 GPa and 87.37 GPa, respectively, as listed in Supplementary Tables 4 and 5.

To shed light on the microscopic mechanism of anomalous compressibility behavior within the (*a*, *b*) plane of Ag_3BO_3, the most intuitive way is to trace the bond length and angle evolution with respect to pressure. The size of the *a*/*b*-axis is determined by the size of [BO_3] groups and the O-Ag-O bar projection along them [Supplementary Figure 5] and can be expressed by the following formula:

$$a = \frac{5}{2} \times l_{B-O} + \frac{4}{3}\sqrt{3} \times \sqrt{{l_{Ag-O1}}^2 + {l_{Ag-O2}}^2 - 2 \times l_{Ag-O1} \times l_{Ag-O2} \times cos\gamma} \times cos\theta \quad (1)$$

in which γ and θ are the angle ∠O-Ag-O and the angle between the O-Ag-O bar and (*a*, *b*) plane, respectively, and $l_{Ag\text{-}O}$ is the bond length between Ag and O. Due to the restriction of symmetry, the Ag-O1 is equivalent to Ag-O2 in Ag_3BO_3-*I*. In Ag_3BO_3-*I*, as the pressure increases from 0 to 10 GPa, the length of B-O bond in planar [BO_3] groups and Ag-O bond in O-Ag-O bars shrink from 1.36648 to 1.35554 Å (by -0.8%) and from 2.14276 to 2.10956 Å (by -1.5%), respectively [Figure 4A and Supplementary Table 6]. Meanwhile, the angle ∠O-Ag-O in the O-Ag-O bar decreases from 133.792° to 132.190° (by -1.2%). All of these structural modifications lead to the contraction of the *a*/*b*-axis. However, the angle between the O-Ag-O bar and (*a*, *b*) plane decreases from 30.654° to 29.457° (by -3.9%), which expands their projection onto the *a*/*b*-axis. These two effects subtlely counterbalance with each other and give rise to the invariant size of the *a*/*b*-axis in response to pressure, i.e., the ZAC within the (*a*, *b*) plane [Figure 4B]. For Ag_3BO_3-*II*, in the pressure range of 0 to 4 GPa, the length of B-O bonds in [BO_3] groups, Ag-O1 and Ag-O2 bonds in the O-Ag-O bar experience contraction from 1.36840 to 1.36267 Å (by -0.4%), from 2.09401 to 2.08012 Å (by -0.7%), and from 2.09607 to 2.08375 Å (by -0.6%), respectively [Figure 4C and Supplementary Table 7]. However, different from Ag_3BO_3-*I*, the angle of ∠O-Ag-O only shrinks from 176.406° to 176.210° (by -0.1%), which does not contribute to the contraction of the O-Ag-O bar. Due to the almost absence of ∠O-Ag-O decreasing, the overall contraction effect of the *a*/*b*-axis is suppressed by the expansion induced by the decrease of the angle between the O-Ag-O bar and (*a*, *b*) plane (from 29.410° to 28.286°, by -3.8%), giving rise to the net expansion response, i.e., NAC of the (*a*, *b*) plane [Figure 4D]. Further, as the pressure mounts from 4 to 10 GPa, the contractions of B-O, Ag-O1, and Ag-O2 bond are enhanced and change from 1.36267 to 1.35485 Å (by -0.6%), from 2.08012 to 2.06086 Å (by -0.9%), and from 2.08375 to 2.06665 Å (by -0.8%), respectively. Similar to the behavior in the range of 0~4 GPa, the angle of ∠O-Ag-O experiences a very tiny change (from 176.210° to 176.106°, less than -0.1%). However, the modification of the angle between the O-Ag-O bar and the (*a*, *b*) plane is weakened in comparison with the value of 3.8% from 0 to 4 GPa and only decreases from 28.286° to 27.414° (by -3.1%). This makes the competition between the contraction and expansion of the *a*/*b*-axis return to the balance and leads to the ZAC response in the pressure range of 4~10 GPa, as Ag_3BO_3-*I*. In "wine-rack" architecture, the opening degree of the framework determines the magnitude of pressure-induced expansion effects[36]. Benefited from its larger structural openness endowed by the O-Ag-O chain closer to the linear configuration than Ag_3BO_3-*I*, at low pressure (0~4 GPa), the prominent expansion effect from inclination of O-Ag-O chain leads to the manifestation of NAC in Ag_3BO_3-*II*, as elucidated in Figure 4D. With the structural densification under pressure, such an expansion effect is gradually weakened, and its counterbalance with the contraction effect triggers the occurrence of ZAC from 4 to 10 GPa. Therefore, the different pressure responses between Ag_3BO_3-*I* and Ag_3BO_3-*II*, as well as that between low-pressure and high-pressure phases of Ag_3BO_3-*II*, could be attributed to the structural openness degree determined by the ∠O-Ag-O angle and pressure-induced structure densification.

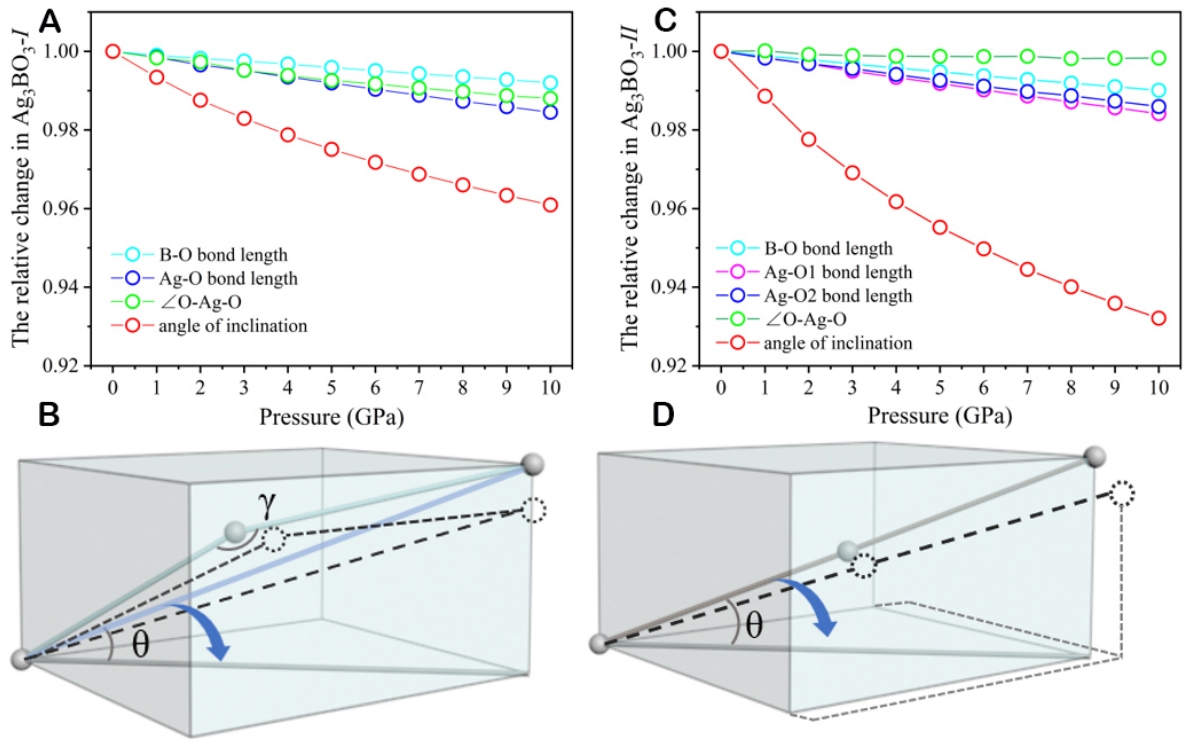

Figure 4. The structural modification of Ag_3BO_3-*I* and Ag_3BO_3-*II* under pressure. (A) The relative change of bond length and angle in Ag_3BO_3-*I*; (B) The schematic of ZAC in Ag_3BO_3-*I*; (C) The relative change of bond length and angle in Ag_3BO_3-*II*; (D) The schematic of NAC in Ag_3BO_3-*II*.

CONCLUSIONS

In summary, through a quantified elaboration, the transition across 45° for the angle between the bar and principal axis governs the occurring direction of expansion effect in the "wine-rack" architecture. Accordingly, through a structural screening in the planar coordination system, the "wine-rack" structure-driven NAC and ZAC were theoretically predicted in Ag_3BO_3-*I* and Ag_3BO_3-*II*. Analysis of bond lengths and bond angles ascribes to the occurrence of abnormal compressibility to the competitive effect between the shrinkage effect from bond length/angle contraction and the expansion effect from inclination angles between the O-Ag-O bar and (*a*, *b*) plane. By virtue of large structure openness generated by linear O-Ag-O coordination, the strong expansion effect promotes the occurrence of the NAC of Ag_3BO_3-*II* in the low-pressure range of 0~4 GPa, while the ZAC in Ag_3BO_3-*I* and Ag_3BO_3-*II* in the pressure range of 4~10 GPa is ascribed to the subtle counterbalance between these shrinkage and expansion effects. The work establishes a quantified relation between the atomic coordination and expansion response in "wine-rack" architecture under pressure. It will bring continuous discovery of the material with anomalous mechanical properties.

DECLARATIONS

Acknowledgments

The authors acknowledge Zhuohong Yin for useful discussions.

Authors' contributions

Made substantial contributions to the conception and design of the study and performed data analysis and interpretation: Zhang X

Made assistant contributions to the calculation method: Liu Y, Wang N
Provided administrative, technical, and material support: Jiang X, Lin Z

Availability of data and materials
Relative data has been published as Supplementary Material in the journal.

Financial support and sponsorship
This work was supported by the National Scientific Foundations of China (Grants 12274425, 11974360, T2222017, and 22133004) and the CAS Project for Young Scientists in Basic Research (YSBR-024).

Conflicts of interest
All authors declared that there are no conflicts of interest.

Ethical approval and consent to participate
Not applicable.

Consent for publication
Not applicable.

REFERENCES
1. Grima JN, Caruana-Gauci R. Mechanical metamaterials: materials that push back. *Nat Mater* 2012;11:565-6. DOI PubMed
2. Baughman RH. Auxetic materials: avoiding the shrink. *Nature* 2003;425:667. DOI PubMed
3. Baughman RH, Stafstrom S, Cui C, Dantas SO. Materials with negative compressibilities in one or more dimensions. *Science* 1998;279:1522-4. DOI
4. Cairns AB, Goodwin AL. Negative linear compressibility. *Phys Chem Chem Phys* 2015;17:20449-65. DOI PubMed
5. Jiang X, Molokeev MS, Dong L, et al. Anomalous mechanical materials squeezing three-dimensional volume compressibility into one dimension. *Nat Commun* 2020;11:5593. DOI PubMed PMC
6. Lu Y, Yan H, Huang E, Chen B. Persistent negative compressibility coupled to optical modulation in empty-perovskite $TiOF_2$. *J Phys Chem C* 2021;125:8869-75. DOI
7. Yu Y, Zeng Q, Chen Y, Jiang L, Wang K, Zou B. Extraordinarily persistent zero linear compressibility in metal-organic framework MIL-122(In). *ACS Mater Lett* 2020;2:519-23. DOI
8. Rejnhardt P, Zaręba JK, Katrusiak A, Daszkiewicz M. Deuteration-enhanced negative thermal expansion and negative area compressibility in a three-dimensional hydrogen bonded network. *Chem Mater* 2023;35:5160-7. DOI
9. Cairns AB, Catafesta J, Levelut C, et al. Giant negative linear compressibility in zinc dicyanoaurate. *Nat Mater* 2013;12:212-6. DOI
10. Zhao Y, Fan C, Pei C, et al. Colossal negative linear compressibility in porous organic salts. *J Am Chem Soc* 2020;142:3593-9. DOI
11. Jiang D, Wen T, Song H, et al. Intrinsic zero-linear and zero-area compressibilities over an ultrawide pressure range within a gear-spring structure. *CCS Chem* 2022;4:3246-53. DOI
12. Zeng Q, Wang K, Zou B. Near zero area compressibility in a perovskite-like metal-organic frameworks $[C(NH_2)_3][Cd(HCOO)_3]$. *ACS Appl Mater Interfaces* 2018;10:23481-4. DOI
13. Sun ME, Wang Y, Wang F, et al. Chirality-dependent structural transformation in chiral 2D perovskites under high pressure. *J Am Chem Soc* 2023;145:8908-16. DOI
14. Qiu W, Zeng Q, Li C, Hao J, Li Y. Theoretical investigation of zero linear compressibility on metal squarates MC_4O_4 (M = Pb and Ba). *J Phys Chem C* 2023;127:9957-63. DOI
15. Mączka M, Sobczak S, Ratajczyk P, et al. Pressure-driven phase transition in two-dimensional perovskite MHy_2PbBr_4. *Chem Mater* 2022;34:7867-77. DOI
16. Jiang X, Luo S, Kang L, et al. Isotropic negative area compressibility over large pressure range in potassium beryllium fluoroborate and its potential applications in deep ultraviolet region. *Adv Mater* 2015;27:4851-7. DOI
17. Zhang Y, Yao M, Du M, et al. Negative volume compressibility in $Sc_3N@C_{80}$-cubane cocrystal with charge transfer. *J Am Chem Soc* 2020;142:7584-90. DOI
18. Tortora M, Zajdel P, Lowe AR, et al. Giant negative compressibility by liquid intrusion into superhydrophobic flexible nanoporous frameworks. *Nano Lett* 2021;21:2848-53. DOI PubMed PMC

19. Occelli F, Loubeyre P, LeToullec R. Properties of diamond under hydrostatic pressures up to 140 GPa. *Nat Mater* 2003;2:151-4. DOI PubMed
20. Jiang D, Wen T, Guo Y, et al. Reentrant negative linear compressibility in MIL-53(Al) over an ultrawide pressure range. *Chem Mater* 2022;34:2764-70. DOI
21. Ghosh PS, Ponomareva I. Negative linear compressibility in organic-inorganic hybrid perovskite $[NH_2NH_3]X(HCOO)_3$ (X = Mn, Fe, Co). *J Phys Chem Lett* 2022;13:3143-9. DOI
22. Hodgson SA, Adamson J, Hunt SJ, et al. Negative area compressibility in silver(I) tricyanomethanide. *Chem Commun* 2014;50:5264-6. DOI
23. Goodwin AL, Keen DA, Tucker MG. Large negative linear compressibility of $Ag_3[Co(CN)_6]$. *Proc Natl Acad Sci USA* 2008;105:18708-13. DOI PubMed PMC
24. Kamali K, Ravi C, Ravindran TR, Sarguna RM, Sairam TN, Kaur G. Linear compressibility and thermal expansion of $KMn[Ag(CN)_2]_3$ studied by raman spectroscopy and first-principles calculations. *J Phys Chem C* 2013;117:25704-13. DOI
25. Cai W, Katrusiak A. Conformationally assisted negative area compression in methyl benzoate. *J Phys Chem C* 2013;117:21460-5. DOI
26. Jiang X, Yang Y, Molokeev MS, et al. Zero linear compressibility in nondense borates with a "Lu-Ban Stool"-like structure. *Adv Mater* 2018;30:e1801313. DOI
27. Clark SJ, Segall MD, Pickard CJ, et al. First principles methods using CASTEP. *Z Kristallogr* 2005;220:567-70. DOI
28. Baroni S, de Gironcoli S, Dal Corso A, Giannozzi P. Phonons and related crystal properties from density-functional perturbation theory. *Rev Mod Phys* 2001;73:515. DOI
29. Perdew JP, Zunger A. Self-interaction correction to density-functional approximations for many-electron systems. *Phys Rev B* 1981;23:5048. DOI
30. Ceperley DM, Alder BJ. Ground-state of the electron-gas by a stochastic method. *Phys Rev Lett* 1980;45:566. DOI
31. Vanderbilt D. Soft self-consistent pseudopotentials in a generalized eigenvalue formalism. *Phys Rev B Condens Matter* 1990;41:7892. DOI
32. Pfrommer BG, Côté M, Louie SG, Cohen ML. Relaxation of crystals with the quasi-newton method. *J Comput Phys* 1997;131:233-40. DOI
33. Cliffe MJ, Goodwin AL. PASCal*:* a principal axis strain calculator for thermal expansion and compressibility determination. *J Appl Cryst* 2012;45:1321-9. DOI
34. Jansen M, Scheld W. Silber(I)-orthoborat. *Z Anorg Allg Chem* 1981;477:85-9. DOI
35. Jansen M, Brachtel G. Ag_3BO_3-II, eine neue form von silber(I)-orthoborat. *Z Anorg Allg Chem* 1982;489:42-6. DOI
36. Serra-Crespo P, Dikhtiarenko A, Stavitski E, et al. Experimental evidence of negative linear compressibility in the MIL-53 metal-organic framework family. *CrystEngComm* 2015;17:276-80. DOI PubMed PMC